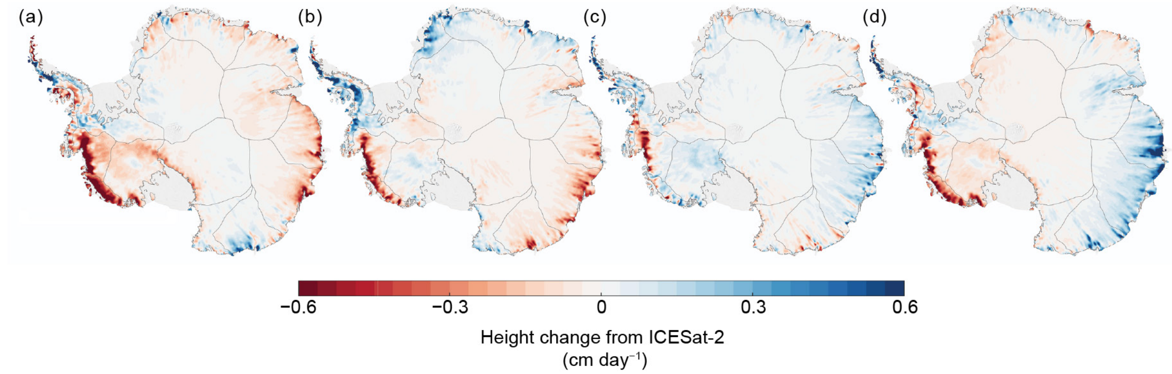

Fig. 6.10. Maps of height change (cm day^{-1}) from ICESat-2 for (a) Nov 2020–Feb 2021, (b) Feb–May 2021, (c) May–Aug 2021, and (d) Aug–Nov 2021. Dates represent the central month of each 3-month ICESat-2 data acquisition cycle.

To examine seasonal variability, we also derived height changes from ICESat-2 at 3-month intervals between November 2020 and November 2021 period using the technique described above for deriving the annual height change map (Fig. 6.10). Although data from the GRACE-FO mission were available at monthly intervals during this period, a small seasonal bias in the AIS mass change signal has been noticed in the GRACE-FO data, which is due to the accelerometer transplant calibration (the accelerometer on one spacecraft is currently not used due to noise; Harvey et al. 2022). This bias is related to the orbital beta-angle, and thus affects the seasonal variations only. The mission's Science Data System has developed an updated accelerometer calibration that removes this seasonal bias in the next data release (planned for boreal spring 2022; F. Landerer, person. comm.). Therefore, we only include annual estimates of ice sheet mass loss from GRACE-FO in this report. Many of the spatial patterns of increases in height across Antarctica correspond well with patterns of positive surface mass balance anomalies reported in 2020 (see Fig. 6.5b). For example, large increases in height over Wilkes Land, East Antarctica, during August–November (Fig. 6.10d) coincided with increases in the frequency of landfalling atmospheric rivers (Adusumilli et al. 2021) during this period (see Fig. 6.6d). This further suggests a major contribution of surface processes in driving seasonal height and mass changes. Meanwhile, decreases in height continued to dominate coastal West Antarctica for all of 2021.

f. Sea ice extent, concentration, and seasonality—P. Reid, S. Stammerjohn, R. A. Massom, S. Barreira, T. Scambos, and J. L. Lieser

During 2021, and following on from 2020, net Antarctic sea ice coverage continued to exhibit strong variability (Fig. 6.11a), with distinct regional and seasonal contributions (Fig. 6.11b). The year began with below-average overall sea ice extent (SIE) in January through February (Fig. 6.11a), compared to the 1991–2020 average, but abruptly switched to above average in late February where it remained almost continuously until early September. Sea ice then retreated at rates faster than average, with net SIE at ~1.5×10^6 km^2 below average in late December. Annual daily minimum SIE occurred on 22 February (2.68×10^6 km^2), which was slightly below average, while the annual daily maximum (18.79×10^6 km^2) was slightly above average but very early (30 August)—the second earliest daily maximum on record. Sea ice area (SIA), which is the product of SIE and concentration, followed a similar overall pattern to SIE but attained near record-high levels in late August (second highest on record), before plummeting to record-low daily values during parts of October and December. A new monthly-mean low SIA (5.45×10^6 km^2) was recorded for December. In terms of regional contributions, the western Weddell, Bellingshausen, and Ross Seas sectors generally experienced smaller-than-average SIE through much of 2021, whereas the Amundsen Sea sector recorded larger-than-average SIE through the year.

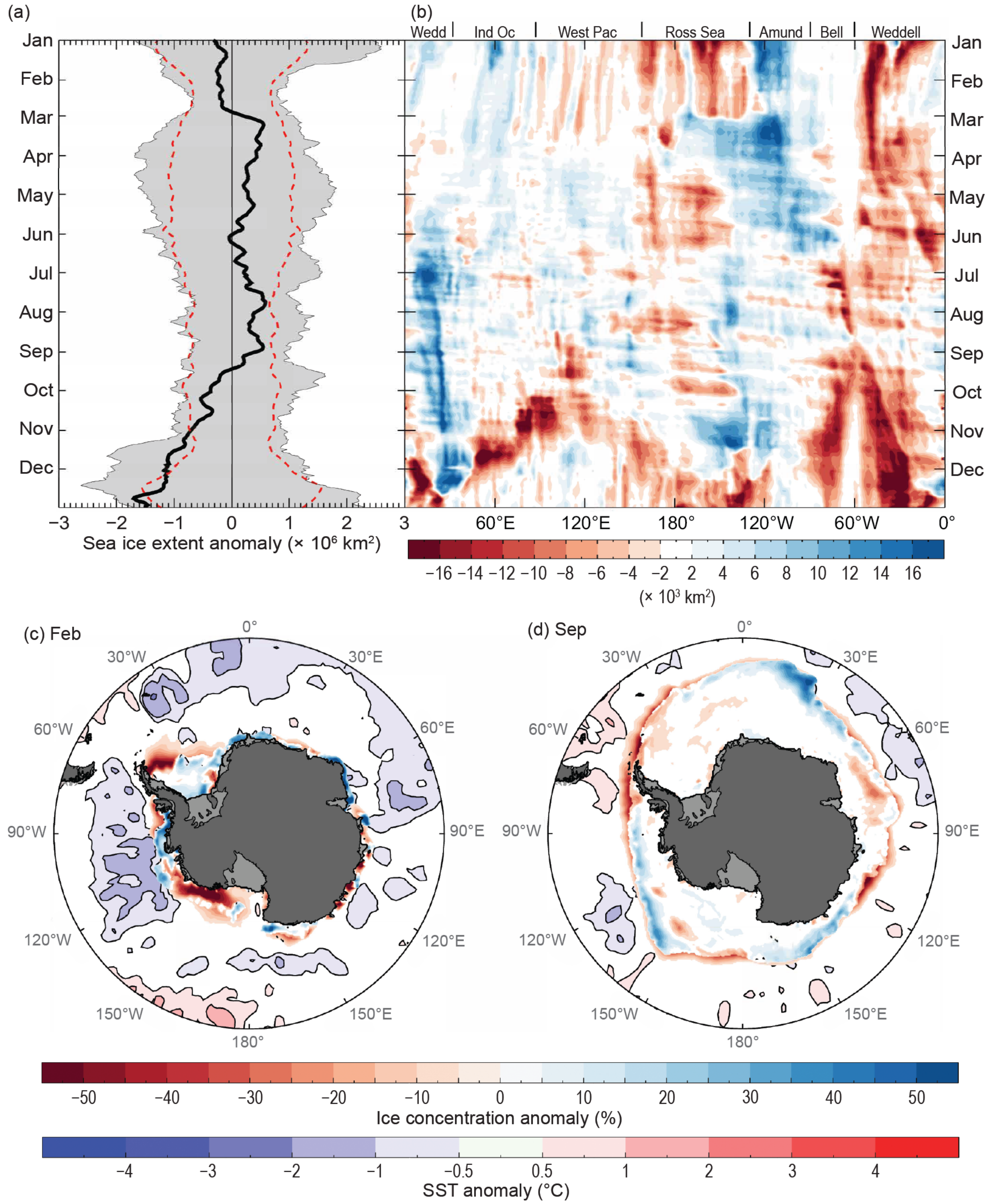

Fig. 6.11. (a) Time series of net daily SIE anomaly (× 10^6 km^2) for 2021 (solid black line) based on 1991–2020 climatology. The gray shading represents the historical (1979–2020) daily SIE anomaly. (b) Hovmöller (time–longitude) representation of daily SIE anomaly (× 10^3 km^2 per degree of longitude) for 2021. Maps of sea ice concentration anomaly (%) and SST anomaly (°C; Reynolds et al. 2002; Smith et al. 2008) for (c) Feb 2021 and (d) Sep 2021. Sea ice concentration is based on satellite passive-microwave ice concentration data (Cavalieri et al. 1996, updated annually, for climatology; Maslanik and Stroeve 1999), for the 2021 sea ice concentration. See Fig. 6.1 for relevant place names.

The low values of SIE and area during the early and then latter months of 2021 continue the recent trend towards decreased Antarctic sea ice coverage. Since 2015, 8 of the 12 calendar months have registered record low net Antarctic SIE (Parkinson and DiGirolamo 2021), but there are distinct regional and seasonal components to these events (Parkinson 2019; Stammerjohn and Maksym 2017). Overall, net Antarctic SIE has displayed substantial variability over the last decade, with record high values during 2012–14 (Reid and Massom 2015), followed by several years of low and record low values (Parkinson 2019; Reid et al. 2021). Through much of 2021, atmospheric anomalies were strong and distinct (section 6b), particularly the depth of the Amundsen Sea Low (ASL) from September onwards. However, given the pattern of generally sustained low sea ice coverage since 2016, it is quite probable that there are ocean influences predisposing the sea ice to early retreat (section 6g; Kusahara et al. 2018; Meehl et al. 2019). Below, we discuss four sequential phases of spatio-temporal progressions of Antarctic sea ice in 2021 based on the patterns and changes shown in Figs. 6.11a,b. These four sea ice phases (January–February, March–April, May–August, and September–December) reflect similar patterns in the atmospheric pressure and wind fields (section 6b) and sea surface temperatures (SSTs).

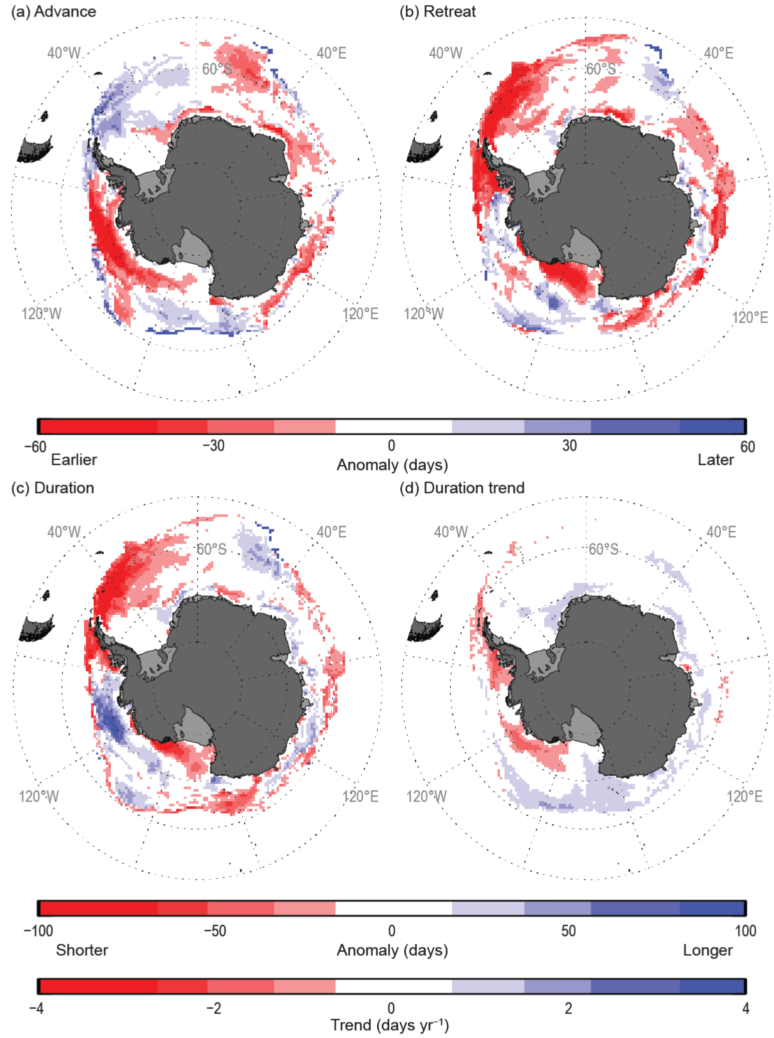

Fig. 6.12. Maps of seasonal sea ice anomalies (days) in 2021 during (a) autumn ice-edge advance, (b) spring ice-edge retreat, (c) winter ice season duration; together with (d) winter ice season duration trend (days yr^{-1}; Stammerjohn et al. 2008). The seasonal anomalies (a–c) are computed against the 1991/92 to 2020/21 climatology; the trend (d) is computed over 1979/80 to 2020/21. (Source: GSFC Bootstrap v3.1 daily data [Comiso 2017] through 31 May 2021, augmented with NASA Team NRTSI daily data [Meier et al. 2021] through 15 Feb 2022.)

As a continuation of the 2020/21 sea ice retreat process, regional patterns of sea ice coverage in January–February 2021 closely followed those of late 2020 (Reid et al. 2021). The regions of persistent high SIE and slower-than-normal seasonal retreat in the Indian Ocean off Dronning Maud Land (~0°–70°E) and in the Amundsen Sea (Fig. 6.11b, and reflected by an earlier advance in Fig. 6.12a) were consistent with below-average SSTs in those regions (Fig. 6.11c; section 6g). These cooler, icier regions were possibly due to the influence of two dominant atmospheric low-pressure anomalies (> 2.5 std. dev. below normal) at ~100°W and 40°E that contributed to the northward advection of cooler air and sea ice. Elsewhere, however, extensive faster-than-average sea ice retreat occurred across much of East Antarctica, the Ross Sea (~70°E–120°W), and the western Weddell Sea (~0°–60°W; Figs. 6.11b,c), leading to a net overall negative SIE anomaly (Fig. 6.11a).

During March, an abrupt change from a negative to a strongly positive anomaly in regional SIE took place in the eastern Ross Sea (Fig. 6.11b) in response to an eastward shift of a well-developed ASL (section 6b). This strong low-pressure anomaly and coincident below-normal SSTs (section

6g) led to rapid sea ice advance in the eastern Ross Sea and across the Amundsen Sea during March–April (Figs. 6.11b, 6.12a). At the same time, an extensive zone of anomalously persistent ice coverage at ~40°–70°E coincided with the southward incursion of a negative SST anomaly associated with a high-pressure anomaly centered on ~25°E. Elsewhere, a relatively slow autumn sea ice advance (Fig. 6.12a) led to negative SIE anomalies across the western Antarctic Peninsula through the Weddell Sea, and also in the western Ross Sea and southwest Pacific Ocean (Fig. 6.11b). In April, circum-Antarctic sea ice was strongly influenced by the development of a zonal wave-3 atmospheric pattern with low-pressure centers at ~40°E, 160°E, and 90°W (see Fig. 6.3e). At this time, the appearance of a predominantly positive SIE anomaly across much of East Antarctica (~0°–130°E) coincided with an increase in cyclonic activity there, and the positive anomaly in the far eastern Ross Sea and Amundsen Sea sector persisted as well. In contrast, SIE remained below average across the western Peninsula and western Weddell Sea and in the Ross Sea region.

During May–July, sea ice conditions were strongly affected by the redevelopment of a deep ASL (a typical La Niña response due to Rossby-wave activity; Yuan 2004) in concert with the persistent, but spatially variable, circumpolar atmospheric zonal wave-3 pattern (section 6b). As part of this pattern, the appearance in May of a deep low-pressure system off Enderby Land (centered on ~45°E) provided strong equatorward air flow that led to enhanced late-autumn sea ice advance (Fig. 6.12a) and a regional positive SIE anomaly that persisted in the eastern limb of the Weddell Gyre through mid-December (Fig. 6.11b). Sea ice advance was also earlier than average across much of East Antarctica west of ~150°E, with persistence of a zonally-extensive positive SIE anomaly from May through July (Fig. 6.11b), likely a result of stronger-than-normal westerly winds due to the combination of low-pressure systems to the south of the sea ice edge and a high-pressure ridge to the north (section 6b). SIE also remained larger than normal in the Amundsen Sea region, but smaller-than-average in the Bellingshausen, western Weddell, and Ross Seas (Fig. 6.11b). This regional pattern of circum-Antarctic anomalies in SIE remained through August, after which there was a development of a more zonally consistent pattern of circumpolar lows (see Fig. 6.3g).

The period of September–December was characterized by an abrupt downturn in overall net SIE around Antarctica (Fig. 6.11a) as a result of zonally-extensive negative SIE anomalies in the Indian and West Pacific Oceans, Bellingshausen through western Weddell Seas, and latterly the Ross Sea (Figs. 6.11b,d). This pattern of anomalously early sea ice retreat (in all sectors apart from the outer eastern Weddell Sea, outer eastern Ross Sea, and portions of the Bellingshausen-Amundsen sector between 80°W and 120°W; Fig. 6.12b) was strongly influenced by a re-emergence and deepening of the ASL in September, which persisted to the end of the year (section 6b). Prevailing warm northerly winds in the eastern part of the ASL particularly impacted the western Peninsula region and western Weddell Sea (~0°–90°W), where SIE was 1–3 std. dev. below the mean from September to the end of the year. Due to the prevalence of cold southerly winds in the western flank of the ASL in the Amundsen and eastern Ross Seas (~90°–150°W), SIE remained predominantly larger than normal until December, at which time it started to retreat rapidly. The exception was the northern Amundsen Sea, where SIE remained above average through to the end of the year (Fig. 6.11b). The continuation of a strong negative SIE anomaly and rapid sea ice retreat in the West Pacific sector in October (Figs. 6.11b, 6.12b) coincided with the development of a major high-pressure anomaly centered offshore at ~170°E. For much of East Antarctica and from September onwards, sea ice retreated rapidly (Fig. 6.12b) and at times regional (~50°–100°E) SIE was 3–4 std. dev. below average. By the end of the year, only the eastern Amundsen Sea and small embayments across East Antarctica showed larger-than-average SIE (not shown).

Large regional anomalies in seasonal advance and retreat combine to produce a distinct pattern of ice season duration anomalies (Fig. 6.12c), with the western Antarctic Peninsula and much of the outer Weddell and inner Ross seas experiencing a much shorter ice season duration by more than 50 days. The shorter ice season along the western Antarctic Peninsula and eastern

Ross Sea are consistent with their long-term trends, in contrast to the ice season anomalies in the Bellingshausen-Amundsen region between 80°W and 120°W and the western Ross Sea, both of which were opposite to their long-term trends (Figs. 6.12 c,d).

g. Southern Ocean—R. L. Beadling, N. M. Freeman, G. A. MacGilchrist, M. Mazloff, J.-R. Shi, A. F. Thompson, and E. Wilson

The Southern Ocean (SO) moderates the climate system as a vast, but variable, sink for anthropogenic heat (Frölicher et al. 2015; Shi et al. 2018) and carbon dioxide (CO_2, Frölicher et al. 2015). Additionally, nutrients upwelled in the subpolar SO and advected northward fertilize three quarters of global ocean biological productivity (Sarmiento et al. 2004). Motivated by their imprint on the climate system through their role in the SO heat and carbon budget, we present 2021 anomalies of SO sea surface temperature (SST), mixed layer (ML) properties, ocean heat content (OHC), and surface chlorophyll concentration. The state of the SO in 2021 was characterized by zonally-asymmetric SST anomalies, near-record positive anomalies in ML salinity (MLS) and ML depth (MLD) in portions of the SO, a continued increase in ocean heat content (OHC), accelerated upper ocean zonal flow, and near-record summer chlorophyll concentrations.

1) SEA SURFACE TEMPERATURE AND MIXED LAYER PROPERTIES

Southern Ocean SST and ML properties in 2021 are analyzed with respect to the 2004–20 period. Monthly SST data are from the NOAA Optimum Interpolation (OISST) V2 product (Reynolds et al. 2002), while ML properties are from the Argo-based Roemmich-Gilson dataset (Roemmich and Gilson 2009; RG09). We focus on 40°–65°S since this region encapsulates variations around the Antarctic Circumpolar Current (ACC). Following the de Boyer Montegut et al. (2004) threshold method, MLD is defined as the depth at which potential density changes by the threshold value of 0.03 kg m^{-3} relative to the 10-m surface reference value.

In 2021, SO SST anomalies exhibited a distinct zonal asymmetry, with anomalies largely compensating in the zonal mean (Figs. 6.13a,b). Anomalous cooling spanned the central Atlantic to central Indian Oceans and across the eastern Pacific, while anomalous warming was prominent across the western portions of the Pacific and Atlantic. These anomaly patterns are consistent with the Southern Annular Mode (SAM) being in a strongly positive state for much of 2021 (section 6b; Sallée et al. 2010). Zonal-mean MLS approached record highs (~0.02 g kg^{-1}) toward the end of 2021, with large anomalies in the South Atlantic (Figs. 6.13c,d). This may be viewed as a resumption of the higher-than-normal MLS that persisted from 2015 to 2020. Possible factors contributing to the high MLS include the reduction in Antarctic SIE (section 6f), a poleward shift of precipitation away from midlatitudes associated with a more southerly storm track during the positive SAM phase, and a stronger South Atlantic subtropical gyre. A stronger gyre implies increased transport of saline sub-tropical waters to the region. Sea surface height (SSH) maps from Archiving, Validation, and Interpretation of Satellites Oceanographic Data (AVISO; www.aviso.altimetry.fr/duacs/) support a continued (Qu et al. 2019) spin-up of this gyre, with 2021 mean SSH magnitudes ~2 cm greater in the center of the gyre relative to the 1993–2020 climatology (Southern Hemisphere spatially-averaged trend was first removed; not shown here). Distinguishing between these plausible mechanisms would require a thorough salinity budget analysis. Deep winter MLDs (anomalies > 100 m) were found across the southeastern Pacific in 2021 (Fig. 6.13e,f), comparable to the record MLD anomalies that occurred in 2010. Similar to 2010, 2021 was dominated by a positive SAM, which favors deeper winter mixed layers in the southeastern Pacific (Fogt et al. 2011; Sallée et al. 2010) increasing local ocean ventilation and creating conditions conducive to enhanced mode water formation in the region (MacGilchrist et al. 2021; Morrison et al. 2022).